

Jump-Diffusion Approximation of Stochastic Reaction Dynamics: Error bounds and Algorithms

Arnab Ganguly^{1*}, Derya Altıntan^{2,3,4*}, Heinz Koepl⁴

October 1, 2018

Abstract

Biochemical reactions can happen on different time scales and also the abundance of species in these reactions can be very different from each other. Classical approaches, such as deterministic or stochastic approach fail to account for or to exploit this multi-scale nature, respectively. In this paper, we propose a jump-diffusion approximation for multi-scale Markov jump processes that couples the two modeling approaches. An error bound of the proposed approximation is derived and used to partition the reactions into fast and slow sets, where the fast set is simulated by a stochastic differential equation and the slow set is modeled by a discrete chain. The error bound leads to a very efficient dynamic partitioning algorithm which has been implemented for several multi-scale reaction systems. The gain in computational efficiency is illustrated by a realistically sized model of a signal transduction cascade coupled to a gene expression dynamics.

MSC 2010 subject classifications: 60H30, 60J28, 92B05

Keywords: Jump diffusion processes, diffusion approximation, Markov chains, multiscale networks, biochemical reaction networks.

1 Introduction

A biochemical reaction system involves multiple chemical reactions and several molecular species. Recent advances in single cell and single molecule imaging together with

*authors with equal contribution

¹Department of Mathematics, University of Louisville, arnab.ganguly@louisville.edu

²Department of Mathematics, Selçuk University, altintan@selcuk.edu.tr

³Department of Scientific Computing, Middle East Technical University

⁴Department of Electrical Engineering and Information Technology, Technische Universität Darmstadt, heinz.koepl@bcs.tu-darmstadt.de

microfluidic techniques have testified to the random nature of gene expression and protein abundance in single cells [6, 8, 10, 35]. The stochastic nature of a well-mixed biochemical reaction system is most often captured by modeling the dynamics of its species' abundance as a continuous time Markov chain (CTMC) [2]. Popular algorithms for exact simulations of such reaction systems include Gillespie's first and next reaction method [11] and its more efficient variants [12]. These algorithms track every molecular reaction event and thus become computationally expensive when reaction system becomes larger or more complex. For reaction systems involving fast reactions and high copy number of species, substantial gain in simulation speed is often obtained by resorting to approximate algorithms like tau-leaping or Langevin (diffusion) approximation. However, chemical reactions in biological cells occur with varying orders of abundance of molecular species and varying orders of magnitudes of the reaction rates. In these scenarios, suitable hybrid methods need to be implemented to gain speed and efficiency while maintaining the certain level of accuracy.

Typically, in a hybrid model significant computational efficiency is obtained by treating some appropriate species as continuous variables and the others as discrete ones. The first step in this approach involves partitioning the reaction set into "fast" and "slow" reactions. The reason for this partitioning is to simulate the fast set either by Langevin (diffusion) approximation or by ordinary differential equation (ODE) approximation while keeping the discrete Markov chain formulation for the slow ones. The resulting approximate algorithms give rise to hybrid stochastic processes where the species with high copy numbers are treated as continuous variables, while the ones with low copy numbers are kept as discrete variables. The dynamics of the continuous variables then can be seen to be governed by ordinary differential equations or stochastic differential equations punctuated by jumps due to the discrete components.

Based on that idea, different hybrid models have been proposed [7, 16, 31]. For example, in [31], authors separate the reactions into fast and slow groups such that the Langevin equation is used to simulate the dynamics of fast reactions while integral form of the next reaction method is used to describe the behavior of the slow ones. [17] applies a method of conditional moments (MCM) which uses a moment based description for the species with high copy number of molecules while a stochastic description is kept for species with low copy number of molecules. A hybrid representation, that assumes a continuous and deterministic behavior of the conditional expectation of high copy species given the state of species with low copy numbers, is introduced in [19]. In [1], authors proposed three different algorithms for simulating the hybrid systems that solve deterministic equations and trace the stochastic reaction event in the meantime. Different hybrid strategies for solving the chemical master equation are proposed in [18, 20, 28].

Jahnke and Kreim considered in [21] a piecewise deterministic model where species with low copy numbers are considered as discrete stochastic variables and the species with high copy numbers are treated as considered as continuous variables. In such a model a CTMC process describing the evolution of species with low copy number is coupled with ODEs representing the dynamics of high copy species. [21] studied the partial thermodynamic limit of such a system and proved that after suitable scaling the approximate error of the hybrid model in the marginal distributions is of the order M^{-1} , where M is a scaling parameter of the system. The parameter M captures

the abundance of high copy species and is typically chosen such that those species are $O(1)$. However, the partition of the species set is still subjective and it is not immediately clear how to use the result in [21] to form an objective measure for partitioning the species set. Also, it should be noted that the partitioning the species set will have the following effect: a reaction which affects a discrete species and a continuous species will be treated differently in the equations describing the dynamics of the two species. While for the discrete species the number of occurrence of such a reaction will be considered as a stochastic counting process, it will be calculated by a deterministic integral for the continuous species. This might slow down an algorithm which is based on such a partitioning of the species set, as the same quantity is calculated in two different ways. In contrast, the present article considers a hybrid diffusion model where the reaction set is partitioned into slow and fast reactions and most importantly, our approach to the error analysis has the sole goal of devising an objective measure for partitioning the reaction set. Our result is formulated in an efficient hybrid algorithm which itself is able to do the partitioning of the reaction set and also check the validity of the partitioning dynamically over the course of time.

Intuitively, the reaction set with higher propensities will occur at a greater speed and using a diffusion approximation to simulate the occurrence of those reactions will preserve the accuracy of the simulation. However, in existing literature the identification of reactions with higher propensities is often done in a subjective and ad hoc way; one difficulty in the designation process lies within varying magnitudes of different propensities. The higher value of a propensity of a reaction may occur due to its large rate constant or due to high copy number of the reactant species or due to some combination of both the factors. The present article attempts to solve this problem by introducing a scaling parameter N and suitable scaling exponents α_k, β_k to capture the order of variation of the species abundance and magnitudes of the reaction rates. These types of scaled models were previously studied in [22] where the authors used limiting arguments and stochastic averaging techniques for model reduction (also see [23]). The most significant portion of the present paper is a rigorous error analysis aimed toward proper identification of the partitioning of the reaction set into the fast and the slow ones for a given tolerance for error.

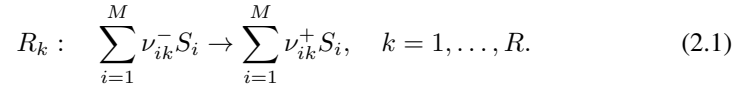
The main theoretical result obtaining the required error bound has been described in Theorem 2.3. The appearance of the different scaling exponents α_k and β_k in the error bound singles out the reactions whose occurrences when simulated by diffusion approximation give the lowest possible error. The methodology forms the backbone of a very accurate dynamic partitioning algorithm described in Algorithm 1. While most of the previous works on hybrid simulation were based on the chemical master equation [17, 28], the present paper uses an approach based on a representation of the state vector by stochastic equations. These types of differential equation representations of the state of the system [2, 9] give deeper insight into the full trajectories of both the exact and the approximating processes in contrast to a chemical master type equation, which only describes the state probabilities at specific time points. The pathwise representations of the processes also allow us to define the error of approximation in a suitable rigorous way, and the corresponding error bound is then derived by proper use of techniques from stochastic analysis.

The rest of the paper is organized as follows. In Section 2, we describe the Markov

chain formulation of the reaction system and the approximating hybrid diffusion model. The pathwise representation of both, the exact and the approximating processes through appropriate stochastic equations are also given. The section also introduces the important scaling exponents required for describing a multi-scale model, and the main error bound is obtained in Theorem 2.3. Section 3 concerns itself with the development of the dynamic partitioning algorithm by utilizing the novel error bound. Section 4 describes a Runge-Kutta integration method for simulating the hybrid diffusion equation, and Section 5 makes proper use of the naturally occurring conservation relations in reaction systems to reduce the dimensionality of the system state and to make the algorithm numerically more robust. Finally, in Section 6, the proposed algorithm is implemented to analyze the Michaelis-Menten kinetics, the Lotka-Volterra model and the important MAPK pathway together with its gene expression.

2 Model Setup and Error Bound

We will consider chemical reaction systems consisting of M chemical species, S_1, \dots, S_M , R reactions, R_1, \dots, R_R



Here, ν_{ik}^- and ν_{ik}^+ respectively denote the number of molecules of the species S_i consumed and created due to one occurrence of reaction R_k . Let $X(t) \in \mathbb{N}^M$ denote the state of the reaction system at time t . If ν_k denote the vector with i -th component $\nu_{ik}^+ - \nu_{ik}^-$, then an occurrence of R_k at time t updates the state by the following equation

$$X(t) = X(t-) + \nu_k.$$

The process X is a CTMC with transition probabilities governed by

$$\mathbb{P}[X(t+h) = x + \nu_k | X(t) = x] = a_k(x)h + o(h),$$

where a_k is the propensity function associated with reaction R_k and is calculated by the law of mass action kinetics in the present article. In other words,

$$a_k(x) = c_k \prod_{i=1}^M \binom{x_i}{\nu_{ik}^-},$$

where c_k is the stochastic reaction rate constant for reaction R_k . A pathwise representation of the process X is given by the following stochastic equation

$$X(t) = X(0) + \sum_{k=1}^R \xi_k \left(\int_0^t a_k(X(s)) ds \right) \nu_k, \quad (2.2)$$

where the ξ_k are independent unit Poisson processes. It should be noted that the quantities $\xi_k(\int_0^t a_k(X(s)) ds)$ count the number of occurrences of the reaction R_k by time

t . (2.2) is an example of a random time change representation in which stochastic equations involve random time changes of other Markov processes (for details, see [9, Chapter 6]). The generator of the the Markov process X is given by

$$\mathcal{A}f(x) = \sum_{k=1}^R a_k(x)(f(x + \nu_k) - f(x)),$$

that is, for a bounded-measurable function f the quantity

$$f(X(t)) - f(X(0)) - \int_0^t \mathcal{A}f(X(s))$$

is a martingale (with respect to the filtration $\{\mathcal{G}_t\}$ defined in (2.5)). Consequently, taking $f(y) = 1_{\{x\}}(y)$, it follows that the probability mass function of $X(t)$ satisfies the following Kolmogorov forward equation (or the master equation in chemical literature)

$$\frac{\partial p(x, t)}{\partial t} = \sum_{k=1}^R [a_k(x - \nu_k)p(x - \nu_k, t) - a_k(x)p(x, t)],$$

where $p(x, t) = \mathbb{P}(X(t) = x)$. Following [22], we next introduce an appropriate scaled process X^N which will be a primary object in our error analysis. In a typical multi-scale model, the abundance of various species in the reaction system can vary over different orders of magnitude. Let $\alpha_i > 0$ and define $\bar{X}_i^N = X_i/N^{\alpha_i}$. The α_i are chosen such that $\bar{X}_i^N = O(1)$; in other words, α_i measures the order magnitude in abundance for species S_i . In a typical reaction system, the stochastic rate constants c_k can also vary over different orders of magnitude. Therefore, with the same spirit we define $d_k = c_k/N^{\beta_k}$ such that $d_k = O(1)$.

Under the above scaling of the state vector and the rate constants, the propensities a_k scale as $a_k(X) = N^{\beta_k + \nu_k^- \cdot \alpha} \lambda_k(\bar{X}^N)$, where $\alpha = (\alpha_1, \dots, \alpha_M)$. For example, for unimolecular reactions $S_1 \rightarrow *$ we get

$$a_1(X) = c_1 X_1 = N^{\beta_1} d_1 N^{\alpha_1} \bar{X}_1^N = N^{\beta_1 + \alpha_1} d_1 \bar{X}_1^N = N^{\beta_1 + \alpha_1} \lambda_1(\bar{X}^N),$$

while for bimolecular reactions of the type $S_1 + S_2 \rightarrow *$ one obtains

$$a_2(X) = c_2 X_1 X_2 = N^{\beta_2 + \alpha_1 + \alpha_2} d_2 \bar{X}_1^N \bar{X}_2^N = N^{\beta_2 + \alpha_1 + \alpha_2} \lambda_2(\bar{X}^N).$$

Note that with these choices of exponents, the functions $\lambda_k(\cdot)$ are $O(1)$. Oftentimes, it is beneficial to scale time as well by $t \rightarrow tN^\gamma$. With all of the above scalings, we look at the process X^N defined by $X^N(t) = \bar{X}^N(tN^\gamma)$. It readily follows from (2.2) that X^N satisfies

$$X^N(t) = X^N(0) + \sum_{k=1}^R \xi_k(N^{\rho_k} \int_0^t \lambda_k(X^N(s)) ds) \nu_k^N, \quad (2.3)$$

where $\rho_k = \gamma + \beta_k + \nu_k^- \cdot \alpha$ and $\nu_{ki}^N = \nu_{ki}/N^{\alpha_i}$.

2.1 Mathematical preliminaries

We start with the following useful lemma.

Lemma 2.1. *Let ξ be a unit Poisson process adapted to a filtration $\{\mathcal{H}_t\}$ and σ_1, σ_2 bounded $\{\mathcal{H}_t\}$ -stopping times. Then*

$$\mathbb{E}[|\xi(\sigma_1) - \xi(\sigma_2)|] = \mathbb{E}[|\sigma_1 - \sigma_2|].$$

Proof. First note that both $\sigma_1 \vee \sigma_2$ and $\sigma_1 \wedge \sigma_2$ are $\{\mathcal{H}_t\}$ -stopping times. Since $\xi(t) - t$ is a $\{\mathcal{H}_t\}$ -martingale, by optional sampling theorem we have

$$\mathbb{E}[\xi(\sigma_1 \wedge \sigma_2)] = \mathbb{E}[\sigma_1 \wedge \sigma_2], \quad \mathbb{E}[\xi(\sigma_1 \vee \sigma_2)] = \mathbb{E}[\sigma_1 \vee \sigma_2].$$

The assertion now follows because

$$\begin{aligned} \mathbb{E}[|\xi(\sigma_1) - \xi(\sigma_2)|] &= \mathbb{E}[\xi(\sigma_1) \vee \xi(\sigma_2) - \xi(\sigma_1) \wedge \xi(\sigma_2)] \\ &= \mathbb{E}[\xi(\sigma_1 \vee \sigma_2)] - \mathbb{E}[\xi(\sigma_1 \wedge \sigma_2)] = \mathbb{E}[\sigma_1 \vee \sigma_2] - \mathbb{E}[\sigma_1 \wedge \sigma_2] \\ &= \mathbb{E}[|\sigma_1 - \sigma_2|]. \end{aligned}$$

Here the second equality holds because ξ is an increasing process. \square

Now let $\xi_k, k = 1, \dots, R$ be independent unit Poisson processes and define the filtration

$$\mathcal{F}_{\tilde{u}}^l \equiv \sigma\{\xi_k(s_k) : 0 \leq s_k \leq u_k, k = 1, \dots, R\},$$

where $\tilde{u} = (u_1, u_2, \dots, u_R)$ is a multi-index. Let $\mathcal{F}_{\tilde{u}}$ be the completion of the filtration of $\mathcal{F}_{\tilde{u}}^l$. With X as in (2.2), define

$$\tau_k(t) = \int_0^t a_k(X(s)) ds.$$

Then $\tau(t) = (\tau_1(t), \dots, \tau_R(t))$ is a multi-parameter $\{\mathcal{F}_{\tilde{u}}\}$ -stopping time (see [9, Chapter 6]). Consequently, for two intensity functions a_k^1, a_k^2 and the corresponding processes X^1, X^2 , the following is an outcome of Lemma 2.1:

$$\begin{aligned} \mathbb{E} \left[\left| \xi_k \left(\int_0^t a_k^1(X^1(s)) ds \right) - |\xi_k \left(\int_0^t a_k^2(X^2(s)) ds \right) \right| \right] \\ = \mathbb{E} \left[\left| \int_0^t a_k^1(X^1(s)) ds - \int_0^t a_k^2(X^2(s)) ds \right| \right]. \end{aligned} \quad (2.4)$$

Next define the filtration $\{\mathcal{G}_t\}$ by

$$\mathcal{G}_t = \mathcal{F}_{\tau(t)}. \quad (2.5)$$

Then notice that by the optional sampling theorem, for each k , $\tilde{\xi}_k(\tau_k(t)) = \xi_k(\tau_k(t)) - \tau_k(t)$ is a $\{\mathcal{G}_t\}$ -martingale.

2.2 Hybrid Diffusion Models

After a possible renaming of the species, assume that reaction R_1 is of the type $S_1 + S_2 \rightarrow S_3$. The goal of this section is to compute a bound for the error when the reaction R_1 is simulated according to a diffusion approximation. At the process level, this typically means that we are replacing the process $\xi_1(t)$ with $W_1(t) + t$, where W_1 is a standard Brownian motion. With this change, the approximating process Z^N satisfies the equation

$$\begin{aligned} Z^N(t) = & X^N(0) + N^{\rho_1} \int_0^t \lambda_1(Z^N(s)) ds \nu_1^N + W_1(N^{\rho_1} \int_0^t \lambda_1(Z^N(s)) ds) \nu_1^N \\ & + \sum_{k>1} \xi_k(N^{\rho_k} \int_0^t \lambda_k(Z^N(s)) ds) \nu_k^N. \end{aligned}$$

The goal of this section is to bound the error $e(t) = \mathbb{E}|X^N(t) - Z^N(t)|$. It should be noted that the error e depends on the coupling between the processes X^N and Z^N . In particular, this means that e will depend on the construction of the Brownian motion W_1 . The following lemma proves the existence of a Brownian motion W_1 on the same probability space as ξ_1 (see [9, Chapter 11, Section 3]).

Lemma 2.2. *There exists a Brownian motion W_1 on the same probability space as ξ_1 such that W_1 is independent of ξ_k , $k \neq 1$*

$$\sup_t \frac{|\tilde{\xi}_1(t) - W_1(t)|}{\log(2 \vee t)} < \infty,$$

where $\tilde{\xi}_1(t) = \xi_1(t) - t$ denotes the centered Poisson process. Furthermore, for $\delta, \kappa > 0$, there exist constants $\theta, K, C > 0$ such that

$$\mathbb{P} \left[\sup_{t \leq \delta n} |\tilde{\xi}_1(t) - W_1(t)| > C \log n + x \right] \leq K n^{-\kappa} e^{-\theta x}.$$

Let

$$\mathcal{R}_k = \{i : \nu_{ik} \neq 0\}. \quad (2.6)$$

Notice that for each k , \mathcal{R}_k keeps track of the species involved in reaction R_k . We are now ready to state our main result.

Theorem 2.3. *Let X^N be given by (2.3) and Z^N by*

$$\begin{aligned} Z^N(t) = & X^N(0) + N^{\rho_1} \int_0^t \lambda_1(Z^N(s)) ds \nu_1^N + W_1(N^{\rho_1} \int_0^t \lambda_1(Z^N(s)) ds) \nu_1^N \\ & + \sum_{k>1} \xi_k(N^{\rho_k} \int_0^t \lambda_k(Z^N(s)) ds) \nu_k^N, \end{aligned}$$

where W_1 is a standard Brownian motion independent of the ξ_k as given by Lemma 2.2. Assume that the λ_k are Lipschitz continuous with Lipschitz constant L_k and $\sup_x \lambda_k(x) \leq \bar{\lambda}_k$. Let $|\nu_k^N| = O(N^{-m_k}) = O(\sum_{i \in \mathcal{R}_k} \frac{1}{N^{\alpha_i}})$. Then,

$$\sup_{t \leq T} \mathbb{E}|X^N(t) - Z^N(t)| \leq C_N(C' \log N^{\rho_1} / N^{m_1} + K'' / N^{2\rho_1 + m_1}), \quad (2.7)$$

where C_N is a constant which remains the same no matter which reaction is simulated by a diffusion approximation.

Proof. Notice that for $i = 1, 2, 3$

$$\begin{aligned} Z_i^N(t) &= X_i^N(0) + N^{\rho_1} \int_0^t \lambda_1(Z^N(s)) ds \nu_{1i}^N + W_1(N^{\rho_1} \int_0^t \lambda_1(Z^N(s)) ds) \nu_{1i}^N \\ &\quad + \sum_{k>1} \xi_k(N^{\rho_k} \int_0^t \lambda_k(Z^N(s)) ds) \nu_{ki}^N, \end{aligned}$$

and for $i > 3$

$$Z_i^N(t) = X_i^N(0) + \sum_{k>1} \xi_k(N^{\rho_k} \int_0^t \lambda_k(Z^N(s)) ds) \nu_{ki}^N.$$

Let $\tilde{\xi}$ denote the centered Poisson process. Observe that for $i = 1, 2, 3$,

$$\begin{aligned} |X_i^N(t) - Z_i^N(t)| &\leq N^{\rho_1} \left| \int_0^t (\lambda_1(X^N(s)) - \lambda_1(Z^N(s))) ds \right| |\nu_{1i}^N| \\ &\quad + \left| \tilde{\xi}_1(N^{\rho_1} \int_0^t \lambda_1(X^N(s)) ds) - W_1(N^{\rho_1} \int_0^t \lambda_1(Z^N(s)) ds) \right| |\nu_{1i}^N| \\ &\quad + \sum_{k>1} \left| \xi_k(N^{\rho_k} \int_0^t \lambda_k(X^N(s)) ds) - \xi_k(N^{\rho_k} \int_0^t \lambda_k(Z^N(s)) ds) \right| |\nu_{ki}^N| \\ &= A + B + C. \end{aligned} \quad (2.8)$$

Note that by (2.4)

$$\begin{aligned} \mathbb{E}[C] &\leq \sum_{k>1} N^{\rho_k} |\nu_{ki}^N| \mathbb{E} \left| \int_0^t (\lambda_k(X^N(s)) - \lambda_k(Z^N(s))) ds \right| \\ &\leq \sum_{k>1} N^{\rho_k} |\nu_{ki}^N| L_k \int_0^t \mathbb{E}|X^N(s) - Z^N(s)| ds, \end{aligned}$$

where L_k is the Lipschitz constant for λ_k . Also, it is immediate that

$$\mathbb{E}[A] \leq N^{\rho_1} |\nu_{1i}^N| L_1 \int_0^t \mathbb{E}|X^N(s) - Z^N(s)| ds.$$

Next, observe that

$$\begin{aligned} B &\leq |\tilde{\xi}_1(N^{\rho_1} \int_0^t \lambda_1(X^N(s))ds) - \tilde{\xi}_1(N^{\rho_1} \int_0^t \lambda_1(Z^N(s))ds)| |\nu_{1i}^N| \\ &\quad + |\tilde{\xi}_1(N^{\rho_1} \int_0^t \lambda_1(Z^N(s))ds) - W_1(N^{\rho_1} \int_0^t \lambda_1(Z^N(s))ds)| |\nu_{1i}^N| \\ &= I + II. \end{aligned}$$

It is easy to see that for some constant C ,

$$\mathbb{E}[I] \leq CN^{\rho_1} |\nu_{1i}^N| L_1 \int_0^t \mathbb{E}|X^N(s) - Z^N(s)| ds.$$

By Lemma 2.2, there exist constants $\gamma, K', C' > 0$ such that

$$II/|\nu_{1i}^N| \leq \sup_{s \leq \bar{\lambda}_1 N^{\rho_1} t} |\tilde{\xi}_1(s) - W_1(s)| \leq C' \log N^{\rho_1} + \Lambda_N,$$

where $\mathbb{P}[\Lambda_N > x] \leq K' e^{-\kappa x} / N^{2\rho_1}$. Notice that

$$\mathbb{E}[\Lambda_N] = \int_0^\infty \mathbb{P}[\Lambda_N > x] dx \leq K' / \kappa N^{2\rho_1}.$$

It follows that

$$\mathbb{E}[II] \leq (C' \log N^{\rho_1} + K'' / N^{2\rho_1}) |\nu_{1i}^N|.$$

For $i > 3$, we have

$$\begin{aligned} \mathbb{E}|X_i^N(t) - Z_i^N(t)| &\leq \sum_{k>1} \mathbb{E}|\xi_k(N^{\rho_k} \int_0^t \lambda_k(X^N(s))ds) - \xi_k(N^{\rho_k} \int_0^t \lambda_k(Z^N(s))ds)| |\nu_{ki}^N| \\ &\leq \sum_{k>1} N^{\rho_k} |\nu_{ki}^N| \mathbb{E} \int_0^t |\lambda_k(X^N(s)) - \lambda_k(Z^N(s))| ds. \end{aligned} \quad (2.9)$$

It follows from (2.8) and (2.9) that after summing over i

$$\begin{aligned} \mathbb{E}|X^N(t) - Z^N(t)| &\leq \left(\sum_{k=1}^R N^{\rho_k} |\nu_k^N| L_k + N^{\rho_1} L_1 |\nu_1^N| C \right) \int_0^t \mathbb{E}|X^N(s) - Z^N(s)| ds \\ &\quad + (C' \log N^{\rho_1} + K'' / N^{2\rho_1}) |\nu_1^N|, \end{aligned}$$

where $|\nu_k^N| = \sum_i |\nu_{ki}^N|$ is the l_1 norm of ν_k^N . Since $|\nu_k^N| = O(1/N^{m_k})$, Gronwall's inequality implies

$$\mathbb{E}|X^N(t) - Z^N(t)| \leq C_N (C' \log N^{\rho_1} / N^{m_1} + K'' / N^{2\rho_1 + m_1}), \quad (2.10)$$

where $C_N = \exp\left(\sum_{k=1}^R N^{\rho_k} |\nu_k^N| L_k t + N^{\rho_1} L_1 |\nu_1^N| C t\right) \leq \exp\left(2 \sum_{k=1}^R N^{\rho_k} |\nu_k^N| L_k t\right)$. \square

Remark 2.4. Typically, for biochemical systems the propensities a_k and hence the λ_k will not be bounded, a condition required in Theorem 2.3. However, for most practical purposes our simulation takes place in a bounded domain, that is, the simulation is stopped if the number of molecules exceed a certain quantity. Hence, the assumption that the propensity functions are bounded remains valid. Specifically, one way to incorporate this feature in our model is to multiply the original propensity function by a cutoff function ensuring that the changed propensity function vanishes outside a bounded region.

Remark 2.5. For simulation purposes, it is often difficult to estimate the strong error $E|X^N(t) - Z^N(t)|$, as it requires proper utilization of the coupling between X^N and Z^N . It is often more convenient to look at a weak error which compares the error between the marginal distribution of X^N and that of Z^N at a time t . For example, depending on the need, a practitioner might want to estimate the weak error given by $|E(X^N(t)) - E(Z^N(t))|$. While this weak error compares the average values of the exact and the approximating processes, it does not shed light on the error at the level of the corresponding probability distributions. This can be accurately captured by the Wasserstein distance

$$d_W(X^N(t), Z^N(t)) = \sup_f \{ |E(f(X^N(t))) - E(f(Z^N(t)))| : f : \mathbb{R}_+^M \rightarrow \mathbb{R}_+, \text{Lip}(f) \leq 1 \}.$$

Here, the supremum is taken over all Lipschitz continuous f , and $\text{Lip}(f)$ denotes the corresponding Lipschitz constant. It is immediate that

$$d_W(X^N(t), Z^N(t)) \leq E|X^N(t) - Z^N(t)|,$$

and the latter quantity can be bounded by the error bound obtained in Theorem 2.3.

3 Simulation Algorithms

The goal of this section is to use the obtained error bound for constructing a fast algorithm for the dynamic partitioning of the reaction set. The objective of such an algorithm is to implement a proper protocol for simulating the fast reactions by diffusion approximations and to switch back to the original exact Gillespie simulation when the conditions for approximation are not met. Furthermore, switching back and forth between exact simulation and diffusion approximation of appropriate reactions will be done dynamically over the course of time.

The error bound in Section 2, was calculated under the assumption that the system consists of a single fast reaction which was then approximated by a diffusion approximation. This can easily be generalized to a system consisting of more than one fast reaction. Analysis of the error bound in (2.7) reveals that it consists of products of two terms, the first term being a constant (in the sense that its value does not depend on which reaction is approximated by diffusion term), while the second term explicitly captures the effect of the specific reaction being approximated. Consequently, it is the

second part of this error bound which is utilized in partitioning the reaction set into the fast and the slow reaction set. The specific mathematical details are outlined below.

It should be noted that the scaling constants N and the exponents ρ_k, m_k , appearing in (2.7), are determined based on the starting initial state of the system. Hence, a key step in the development of an effective algorithm involves rewriting (2.7) in terms of the propensity functions and the number of molecules of species.

Assume that the reaction R_k is simulated by a diffusion approximation and define

$$\Upsilon_k = C' \log N^{\rho_k} / N^{m_k} + K'' / N^{2\rho_k + m_k}. \quad (3.11)$$

Recall that

$$a_k(X) = N^{\rho_k} \lambda_k(X^N),$$

where $\lambda_k(\cdot) = O(1)$. Therefore,

$$a_k(X) = O(N^{\rho_k}). \quad (3.12)$$

Also, $|\nu_k^N| = O(N^{-m_k}) = O(\sum_{i \in \mathcal{R}_k} \frac{1}{N^{\alpha_i}})$. Since, $\bar{X}_i^N = X_i / N^{\alpha_i}$ where $\bar{X}_i^N = O(1)$, we have $\frac{1}{X_i} = O(\frac{1}{N^{\alpha_i}})$ and

$$O(N^{-m_k}) = O(\sum_{i \in \mathcal{R}_k} \frac{1}{X_i}). \quad (3.13)$$

Ignoring the constants C', K'' and using (3.11), (3.12) and (3.13) it follows that the effect of simulating the reaction R_k by a diffusion approximation is essentially captured by

$$\hat{\Upsilon}_k \equiv \sum_{i \in \mathcal{R}_k} \frac{\log a_k(X)}{X_i} + \frac{1}{a_k^2(X) X_i}, \quad (3.14)$$

where \mathcal{R}_k was defined in (2.6). Now given a threshold ε , a reaction R_k is classified as a fast reaction and simulated by diffusion approximation if $\hat{\Upsilon}_k \leq \varepsilon$. $\hat{\Upsilon}_k$ can be considered as an effective estimate of the quantity Υ_k calculated using the ‘‘initial condition’’ of the state. This approach, in particular, introduces a systematic way of partitioning the reaction set into fast and slow reactions based on a user defined threshold over the

course of time. The resulting algorithm is outlined in details in Algorithm 1.

Algorithm 1: Dynamic partitioning algorithm for hybrid diffusion model.

Input: The state vector X , the error bound ε , a discretization time step Δ , stoichiometric matrix $S = \{\nu_{ij}\}$, $i = 1, 2, \dots, M$, $j = 1, 2, \dots, R$, a positive number P to check repartitioning of reactions, end of the simulation time $T > 0$.

Output: The number of molecules of each species in time interval $t \in [0, T]$.

- 1 Set $t = 0, n = 0$.
 - 2 Calculate $\hat{\Upsilon}_k$ for all reactions by using equation (3.14).
 - 3 Partition the reaction set into \mathcal{C} (continuous) and \mathcal{D} (discrete) sets such that for each $R_k \in \mathcal{C}$, $\hat{\Upsilon}_k \leq \varepsilon$ and for each $R_m \in \mathcal{D}$, $\hat{\Upsilon}_m > \varepsilon$.
 - 4 For each $R_m \in \mathcal{D}$, set $T_m = 0$.
 - 5 For each $R_m \in \mathcal{D}$, draw $J_m \sim -\log(z)$, $z \sim \mathcal{U}(0, 1)$.
 - 6 **while** $t < T$ **and** $\sum_{i=1}^R a_i > 0$ **do**
 - 7 $n = n + 1$.
 - 8 For each $R_m \in \mathcal{D}$, calculate $h_m = \frac{(J_m - T_m)}{a_m}$.
 - 9 Choose α such that $h \equiv h_\alpha \equiv \min_{R_m \in \mathcal{D}} h_m$.
 - 10 **if** $\Delta > h$ **then**
 - 11 Update X by a suitable numerical scheme for simulating the Langevin dynamics for $R_k \in \mathcal{C}$ until the h .
 - 12 Carry out reaction R_α and update $X = X + \nu_\alpha$.
 - 13 Update $J_\alpha = J_\alpha - \log(u)$, $u \sim \mathcal{U}(0, 1)$.
 - 14 For each $R_m \in \mathcal{D}$, put $T_m = T_m + a_m h$.
 - 15 $t = t + h$.
 - 16 **else**
 - 17 Update X by a suitable numerical scheme for simulating the Langevin dynamics for $R_k \in \mathcal{C}$ until the Δ .
 - 18 For each $R_m \in \mathcal{D}$, $T_m = T_m + a_m \Delta$.
 - 19 $t = t + \Delta$.
 - 20 **end**
 - 21 Recalculate the propensities of all reactions a_k .
 - 22 **if** $n \equiv 0 \pmod{P}$ **then**
 - 23 Recalculate errors of all reactions $\hat{\Upsilon}_k$.
 - 24 Repartition reactions as in Step 3.
 - 25 **end**
 - 26 **end**
-

4 Numerical Scheme for Hybrid Diffusion Models

Suppose that the reaction set is partitioned into a set of fast reactions \mathcal{C} and a set of slow reactions \mathcal{D} . The reactions in \mathcal{C} will be simulated by the diffusion approximation. The resulting approximating state process is given by

$$\begin{aligned} X(t) &= X(0) + \sum_{\ell \in \mathcal{C}} \int_0^t a_\ell(X(s)) ds \nu_\ell + \sum_{\ell \in \mathcal{C}} W_\ell \left(\int_0^t a_\ell(X(s)) ds \right) \nu_\ell \\ &+ \sum_{k \in \mathcal{D}} \xi_k \left(\int_0^t a_k(X(s)) ds \right) \nu_k. \end{aligned} \quad (4.15)$$

Therefore, the evolution of the process is governed by a usual diffusion process punctuated by jumps from the slow reaction set. Specifically, let τ_1 and τ_2 denote two successive of reactions from \mathcal{D} . Then, for $\tau_1 < t < \tau_2$,

$$X(t) = X(\tau_1) + \sum_{\ell \in \mathcal{C}} \int_{\tau_1}^t a_\ell(X(s)) ds \nu_\ell + \sum_{\ell \in \mathcal{C}} W_\ell \left(\int_{\tau_1}^t a_\ell(X(s)) ds \right) \nu_\ell. \quad (4.16)$$

Since the reactants in fast reactions usually involve species with high copy numbers, it is useful to look at their concentration $U(t)$ defined by $U(t) = \Omega^{-1} X(t)$, where Ω is the volume of the reaction compartment and $\tau_1 < t < \tau_2$.

Notice that the propensity function of the reaction R_k satisfies the following relation

$$a_k(X) \approx \Omega \tilde{a}_k(U), \quad (4.17)$$

where $\tilde{a}_k : \mathbb{R}_{\geq 0}^M \rightarrow \mathbb{R}$ is the usual deterministic form of mass action $\tilde{a}_k(U) = \tilde{c}_k \prod_{i=1}^M U_i^{\nu_{ik}}$ where \tilde{c}_k denotes the deterministic rate constant. It should be noted that the above relation is exact for unimolecular reactions and bimolecular reactions of the type $S_1 + S_2 \rightarrow *$, and for reactions of the type $2S_1 \rightarrow *$, the error is of the order $O(\Omega^{-1})$. Consequently, for $\tau_1 < t < \tau_2$, U satisfies

$$U(t) = U(\tau_1) + \sum_{\ell \in \mathcal{C}} \int_{\tau_1}^t \tilde{a}_\ell(U(s)) ds \nu_\ell + \sum_{\ell \in \mathcal{C}} \frac{1}{\Omega} W_\ell \left(\int_{\tau_1}^t \tilde{a}_\ell(U(s)) ds \right) \nu_\ell, \quad (4.18)$$

which is equivalent (in the sense of distribution) to the equation

$$U(t) = U(\tau_1) + \sum_{\ell \in \mathcal{C}} \int_{\tau_1}^t \tilde{a}_\ell(U(s)) ds \nu_\ell + \sum_{\ell \in \mathcal{C}} \frac{1}{\sqrt{\Omega}} \int_{\tau_1}^t \sqrt{\tilde{a}_\ell(U(s))} dB_\ell(s) \nu_\ell. \quad (4.19)$$

Here, the B_ℓ are independent standard Brownian motions. Assume that the set \mathcal{C} has C reactions. Then, notice that

$$dU_i = f_i(U) dt + \frac{1}{\sqrt{\Omega}} \sum_{j=1}^C g_{ij}(U) dB_j, \quad i \in \mathcal{S}_C, \quad (4.20)$$

where S_C denotes the species involved in C ,

$$f_i(U) = \sum_{j=1}^C \nu_{ij} \tilde{a}_j(U), \quad g_{ij}(U) = \nu_{ij} \sqrt{\tilde{a}_j(U)}. \quad (4.21)$$

A trajectory of the above stochastic differential equation is simulated by using the Runge-Kutta method with strong order 2 as proposed in [3]. The first step involves rewriting (4.20) in the equivalent Stratonovich form

$$dU_i = \bar{f}_i(U)dt + \frac{1}{\sqrt{\Omega}} \sum_{j=1}^C g_{ij}(U) \circ dB_j, \quad (4.22)$$

where

$$\bar{f}_i(U) = f_i(U) - \frac{1}{2\sqrt{\Omega}} \sum_{j=1}^M \sum_{k=1}^C g_{jk}(U) \frac{\partial g_{ik}(U)}{\partial U_j}, \quad (4.23)$$

with the symbol \circ denoting the Stratonovich integral. The SDE can be represented in matrix form as

$$dU = (S\tilde{a}(U) - \frac{1}{2\sqrt{\Omega}}Sh(U))dt + \frac{1}{\sqrt{\Omega}}S\gamma(U) \circ dB, \quad (4.24)$$

where $\tilde{a}(U) = (\tilde{a}_1(U), \tilde{a}_2(U), \dots, \tilde{a}_C(U))^T$, $B = (B_1, B_2, \dots, B_C)^T$, $\gamma(U) = \text{diag}(\sqrt{\tilde{a}_1(U)}, \dots, \sqrt{\tilde{a}_C(U)})$, and the entries of the vector $h(U)$ are given by

$$h_k(U) = \sum_{j=1}^M \frac{\partial \tilde{a}_k(U)}{\partial U_j} \nu_{jk}, \quad k = 1, 2, \dots, C.$$

Notice that for unimolecular reactions $S_k \rightarrow *$, we have

$$\frac{\partial \tilde{a}_k(U)}{\partial U_j} = \begin{cases} \tilde{c}_k & \text{if } j = k \\ 0 & \text{if } j \neq k, \end{cases}$$

and for bimolecular reactions $S_k + S_i \rightarrow *$, we obtain

$$\frac{\partial \tilde{a}_k(U)}{\partial U_j} = \begin{cases} \tilde{c}_k U_k & \text{if } j = i \\ \tilde{c}_k U_i & \text{if } j = k. \end{cases}$$

Given $U(\tau_1)$ as the approximate solution at time τ_1 , the four stages explicit Runge-Kutta method with strong order 2 for the Stratonovich problem (4.24) gives the following intermediate values I_s , $s = 1, 2, 3, 4$,

$$\begin{aligned} I_s &= U(\tau_1) + h \sum_{j=1}^{s-1} A_{sj} (S\tilde{a}(I_j) - \frac{1}{2\sqrt{\Omega}}Sh(I_j)) \\ &+ \sum_{j=1}^{s-1} \frac{1}{\sqrt{\Omega}} S\gamma(I_j) (B_{sj}^{(1)} J_1 + B_{sj}^{(2)} \frac{J_{10}}{h}), \end{aligned} \quad (4.25)$$

from which the approximate solution at $\tau_1 + h$ is formed:

$$\begin{aligned}
U(\tau_1 + h) &= U(\tau_1) + h \sum_{j=1}^4 \mu_j (S\tilde{a}(I_j) - \frac{1}{2\sqrt{\Omega}} Sh(I_j)) \\
&+ \sum_{j=1}^4 \frac{1}{\sqrt{\Omega}} S\gamma(I_j) (\eta_j^{(1)} J_1 + \eta_j^{(2)} \frac{J_{10}}{h}).
\end{aligned} \tag{4.26}$$

Here, $A = \{A_{sj}\}$, $B^{(k)} = \{B_{sj}^{(k)}\}$, $s, j \in \{1, 2, 3, 4\}$ are 4×4 matrices of real elements, $\mu = \{\mu_j\}$, $\eta^{(k)} = \{\eta_j^{(k)}\}$, $k = 1, 2$, $j = 1, 2, 3, 4$ are row vectors of real elements and J_1 , J_{10} are $C \times 1$ column vectors of real elements. Here, J_1 denotes the Wiener increment and J_{10} is an approximation for the Stratonovich multiple integral $J = \int \int \circ dB ds$. For details of the Runge-Kutta method with strong order 2 and the expressions for the terms A , $B^{(k)}$, μ , $\eta^{(k)}$, J_1 , J_{10} , $k = 1, 2$, see [3, 25].

The prescribed scheme has strong order 2 but imposes a fixed stepsize that need to be chosen very small if the system is stiff. For such stiff problems, we employ a heuristic to adaptively choose the stepsizes of the Runge-Kutta method for a certain integration accuracy. In order to estimate the stepsizes of the Runge-Kutta method for stochastic differential equations (SDEs), we follow the adaptive stepsize control for the classical Runge-Kutta methods for ODEs. To determine the stepsizes of the Runge-Kutta method with strong order 2 for the Stratonovich problem (4.24), we use just the drift term of (4.24).¹ More specifically, we choose an initial step h and compute two approximate solutions of the drift term with stepsizes h and $h/2$ by using the fourth order classical Runge-Kutta method for ODEs. If the difference of the approximations is smaller than a given tolerance, then we choose h as the stepsize and compute the approximate solution of the whole SDE given by (4.24) by using the Runge-Kutta method with strong order 2. We refer the reader to [14], for more details on the adaptive stepsize algorithms for ODEs.

5 Conversion to Differential Algebraic Form

Mass conservation relations play an important role in biochemical reaction systems. In many models the reaction dynamics dictates conservation of the total amount of two or more species over the course of time. For example, in the Michaelis-Menten model the total quantity of the enzyme and the enzyme-substrate complex is always conserved (see Section 6.1). These constraints can be defined by algebraic equations. As a result, the dynamics of the systems under consideration can be expressed by differential algebraic forms that more generally, preserve the symplectic structure of the model on the constraint manifold [13, 15]. These algebraic relations leads to reduction in the dimensionality of the equation set, which in turn speeds up the simulation. The procedure is detailed below.

The algebraic constraints indicate that $r \equiv \text{Rank}\{S\} < M$, where M is the number of species in the reaction system. The next step involves converting the stoichio-

¹Note that in the Stratonovich form the drift term shows a volume dependency.

metric matrix S into a reduced echelon form by Gauss-Jordan method (see [5, 32] for more ways of reconstructing the equations describing the dynamics of such a reaction system). Specifically, the method gives a permutation matrix $E \in \mathbb{N}^{M \times M}$ (that is, E is a product of elementary matrices) such that

$$ES = \begin{bmatrix} E_I \\ E_D \end{bmatrix} S = \begin{bmatrix} S_I \\ 0 \end{bmatrix}, \quad (5.27)$$

where E_I, E_D are $r \times M$ and $(M - r) \times M$ matrices, respectively. Notice that $S_I \equiv E_I S$ has rank r . Here, $E_D S = 0$ means that E_D can be thought of as the conservation matrix. By (4.24), we have

$$EdU = E(S\tilde{a}(U) - \frac{1}{2\sqrt{\Omega}}Sh(U))dt + \frac{1}{\sqrt{\Omega}}ES\gamma(U) \circ dB, \quad (5.28)$$

and hence,

$$\begin{aligned} \begin{bmatrix} dU_I \\ dU_D \end{bmatrix} &\equiv \begin{bmatrix} E_I dU \\ E_D dU \end{bmatrix} \\ &= \begin{bmatrix} E_I(S\tilde{a}(U) - \frac{1}{2\sqrt{\Omega}}Sh(U))dt + \frac{1}{\sqrt{\Omega}}E_I S\gamma(U) \circ dB \\ E_D(S\tilde{a}(U) - \frac{1}{2\sqrt{\Omega}}Sh(U))dt + \frac{1}{\sqrt{\Omega}}E_D S\gamma(U) \circ dB \end{bmatrix} \\ &= \begin{bmatrix} E_I(S\tilde{a}(U) - \frac{1}{2\sqrt{\Omega}}Sh(U))dt + \frac{1}{\sqrt{\Omega}}E_I S\gamma(U) \circ dB \\ 0 \end{bmatrix}. \end{aligned}$$

It follows that (4.24) can be reduced to

$$dU_I = E_I(S\tilde{a}(U) - \frac{1}{2\sqrt{\Omega}}Sh(U))dt + \frac{1}{\sqrt{\Omega}}E_I S\gamma(U) \circ dB \quad (5.29a)$$

$$U_D = E_D U = C, \quad (5.29b)$$

where C is a constant with respect to time. Now writing

$$E^{-1} = \begin{bmatrix} \Psi \\ \Phi \end{bmatrix},$$

we have $U = \Psi U_I + \Phi U_D = \Psi U_I + \Phi C$, where the last equality is because of (5.29b). Consequently, U_I satisfies

$$\begin{aligned} dU_I &= E_I(S\tilde{a}(\Psi U_I + \Phi C) - \frac{1}{2\sqrt{\Omega}}Sh(\Psi U_I + \Phi C))dt \\ &\quad + \frac{1}{\sqrt{\Omega}}E_I S\gamma(\Psi U_I + \Phi C) \circ dB, \end{aligned}$$

and takes its values in a lower dimensional space compared to the original process U . The trajectories of U_I can now be simulated by the Runge-Kutta method as outlined

in Section 4. Specifically, given $U_I(\tau_1)$, (4.25) gives the following intermediate values for the independent variables

$$I_s = U_I(\tau_1) + h \sum_{j=1}^{s-1} A_{sj} E_I(S\tilde{a}(R_j) - \frac{1}{2\sqrt{\Omega}} Sh(R_j)) \\ + \sum_{j=1}^{s-1} \frac{1}{\sqrt{\Omega}} E_I S\gamma(R_j) (B_{sj}^{(1)} J_1 + B_{sj}^{(2)} \frac{J_{10}}{h}),$$

where $R_s = \Psi I_s + \Phi C$, $s = 1, 2, 3, 4$. Finally, we obtain the approximate values of the independent variables at time $\tau_1 + h$ as follows

$$U_I(\tau_1 + h) = U_I(\tau_1) + h \sum_{j=1}^4 \mu_j E_I(S\tilde{a}(R_j) - \frac{1}{2\sqrt{\Omega}} Sh(R_j)) \\ + \sum_{j=1}^4 \frac{1}{\sqrt{\Omega}} E_I S\gamma(R_j) (\eta_j^{(1)} J_1 + \eta_j^{(2)} \frac{J_{10}}{h}). \quad (5.30)$$

Also, $U(\tau_1 + h)$ can be easily obtained from the following equation:

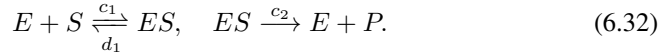
$$U(\tau_1 + h) = \Psi U_I(\tau_1 + h) + \Phi C. \quad (5.31)$$

6 Applications

In this section, the proposed algorithm from Section 3 is applied to the Michaelis-Menten kinetics, the Lotka-Volterra model and a large-scale MAPK pathway model together with its gene expression. The validity of the obtained theoretical error bound for the Michaelis-Menten model is substantiated empirically in Section 6.2. The enormous advantage of our hybrid algorithm over exact stochastic simulation in terms of computational efficiency will be demonstrated in Section 6.4 by considering the complex MAPK pathway.

6.1 The Michaelis-Menten Model

The well known Michaelis-Menten model for enzymatic substrate conversion consists of four species, the enzyme (E), the substrate (S), the enzyme-substrate complex (ES) and the product (P). These species interact via the following reaction channels



The state of the system is defined by the vector of copy numbers $X = (E, S, ES, P)^T$. Notice that the following conservation laws hold

$$E + ES = C_1, \quad S + ES + P = C_2.$$

Here, C_1 and C_2 are constants (with respect to time) and will be considered as dependent variables. In our numerical simulation study, the initial number of molecules is taken as $X(0) = (48, 298, 2, 0)^T$ and the rate constants of reactions R_1, R_2, R_3 are given by $c_1 = 0.02 \text{ molec}^{-1}\text{s}^{-1}$, $d_1 = 0.5 \text{ s}^{-1}$, $c_2 = 0.1 \text{ s}^{-1}$.² The initial number of molecules reveals in the conservation constants $C = (50, 300)^T$.

The system is simulated over the time interval $[0, 100]$ seconds, and the fixed step-size for simulating the continuous SDE part is taken to be $\Delta = 0.3\text{s}$. The relative threshold error for partitioning the reactions is taken to be $\varepsilon = 0.25$, and the reaction set is repartitioned after every $P = 50$ iterations of updating the state vector. As pointed out before, the SDE part of the approximating hybrid diffusion process is simulated by a Runge-Kutta method of strong order 2 as outlined in Section 5. Figure 1 depicts the types of reactions and a single realization of the model when Algorithm 1 is applied. Figure 2 compares the probability distributions and Q-Q plots of the states S and P at time $t = 60\text{s}$ obtained from simulating the exact CTMC model with Gillespie’s algorithm and the hybrid diffusion model with Algorithm 1 of Section 3. It should be observed that the probability distributions and Q-Q plots obtained from the approximate hybrid diffusion algorithm are remarkably close to those obtained from the exact Gillespie algorithm demonstrating the accuracy of our dynamic partitioning algorithm. Evidently, the accuracy can be further increased by lowering the threshold ε of the error bound (3.14). This would lead to partitioning where most reactions for most of the time are treated as discrete reactions.

²Michaelis-Menten model is a classical multi-scale problem because the reversible reaction $E + S \xrightleftharpoons[c_1]{c_2} ES$ is much faster than the reaction $ES \xrightarrow{c_2} E + P$ by orders of magnitude. This situation will lead a static partitioning of the reactions. Therefore, we choose the rate constants of the reaction rates such that we can simulate the model with dynamic partitioning of the reactions.

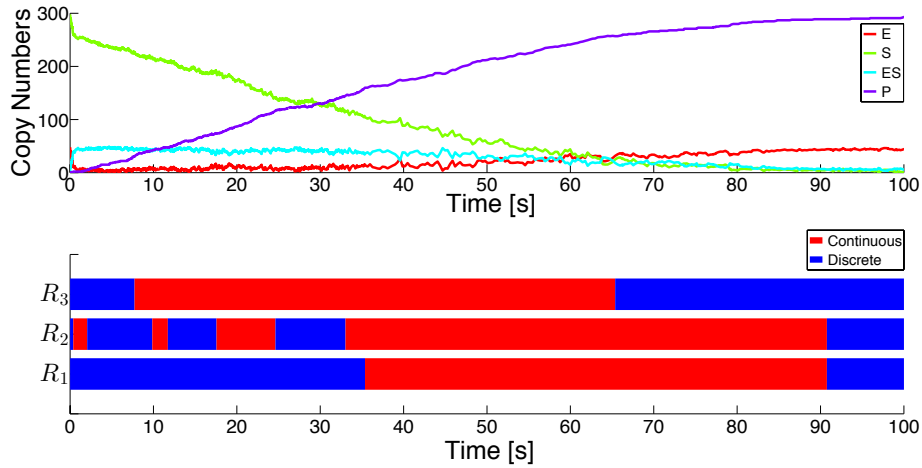


Figure 1: Illustration of the hybrid diffusion algorithm with dynamic partitioning of reaction channels. Upper Panel: A single realization of the Michaelis-Menten model when the fast reactions are modeled by diffusion approximations. Lower Panel: The portions of time when a reaction is treated as fast (continuous) or slow (discrete) as dictated by the error bound (3.14).

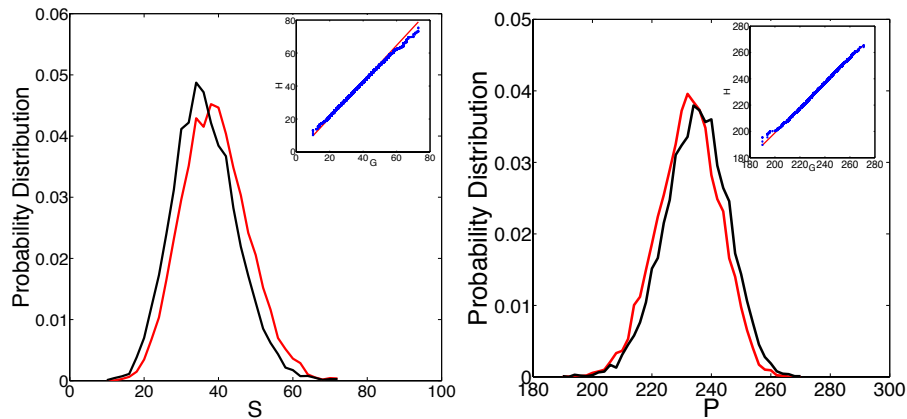


Figure 2: Probability distributions of S (left), P (right) at time $t = 60$ s from 30000 samples constructed with (i) the Gillespie's algorithm (black line) and by (ii) the hybrid diffusion algorithm (red line). Insets show Q-Q plot of 30000 samples comparing the Gillespie's algorithm (G) and the hybrid diffusion algorithm (H).

6.2 Validating the Error Bound

Recall that the error bound obtained in Theorem 2.3 has two parts of which Υ_k , defined by (3.11), captures the effect of treating reaction R_k as a fast reaction and simulating it by a diffusion approximation. It should be noted that Υ_k depends on the initial condition. For an error bound to be meaningful for an appropriate scheme, it is desirable that it is sensitive, meaning that if the actual error increases or decreases, the bound behaves accordingly. Theoretically, in this case this means that for a fixed time interval $[0, t]$, we want Υ_k to be a non-decreasing function of $e_k(t) = |\mathbb{E}[X^N(t)] - \mathbb{E}[Z^N(t)]|$ when they both vary with respect to different initial conditions. Recall that N is a scaling parameter which was determined according to a particular given initial state. The suffix k is used to signify that the reaction R_k is simulated by a diffusion approximation. For a particular reaction system, this could be effectively checked by plotting \hat{e}_k (a Monte-Carlo estimate of e_k) versus $\hat{\Upsilon}_k$ (the Monte-Carlo estimate of Υ_k given by (3.14)) for different initial conditions.

For the present Michaelis-Menten model, R_1 is considered as a fast (continuous) reaction while R_2 and R_3 are kept as slow (discrete) ones (see Section 2.2). The initial values of E , ES and P are kept fixed at $E(0) = 10$, $ES(0) = 30$ and $P(0) = 0$, while the initial values of the substrate S are varied over 9 different values from $\{25, 30, 35, 40, 45, 50, 55, 60, 65\}$. The time interval is taken to be $[0, 1]$ s and the fixed stepsize for simulating the continuous SDE part is taken as $\Delta = 0.1$ s. The rate constants are given by $c_1 = 0.02 \text{ molec}^{-1}\text{s}^{-1}$, $d_1 = 0.5 \text{ s}^{-1}$, $c_2 = 0.1 \text{ s}^{-1}$, for reactions in (6.32). For M realizations of the exact process X^N and the approximating process Z^N , \hat{e}_1 was calculated by the usual Monte-Carlo average:

$$\hat{e}_1 = \sum_{i=1}^4 \left| \frac{1}{M} \sum_{j=1}^M X_{ij}^N(t) - \frac{1}{M} \sum_{j=1}^M Z_{ij}^N(t) \right| \text{ with } t = 1\text{s}, \quad (6.33)$$

where X_{ij}^N , Z_{ij}^N denote the number of molecules of the i -th species for the j -th realization for the corresponding processes. The result presented in Figure 3 demonstrates the desired monotone increasing property of the error bound.

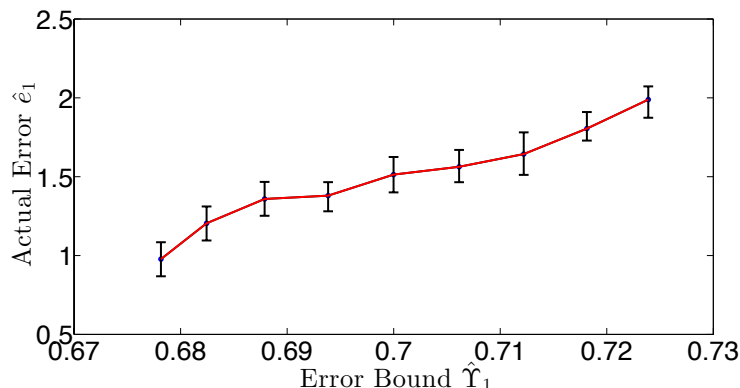
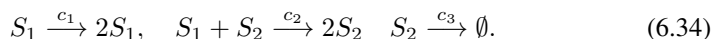


Figure 3: Monotone relation between actual error \hat{e}_1 and the error bound (3.14) for the Michaelis-Menten model (6.32). Monte-Carlo estimates are obtained by the Gillespie’s direct method and by the hybrid diffusion algorithm static partitioning for different initial conditions when R_1 in (6.32) is simulated by a diffusion approximation. We compute the error coming from R_1 through (3.14) (x axis) and the difference of expectations through (6.33) (y axis) for each initial condition for $M = 50000$ realizations at $t = 1$ s. The blue dots denote \hat{e}_1 for initial values and the error bars represent the confidence interval with lower error bound using a percentage of 5% while upper error bound using a percentage of 95%.

6.3 Lotka-Volterra Model

For our next example, we consider the popular Lotka-Volterra model, also known as the predator-prey system. The model describes the dynamics of an abstract environmental system where two animal species interact. Let S_1 and S_2 denote the prey and predator, respectively, the corresponding reaction system is given by



The state of the system is defined by $X(t) \in \mathbb{Z}_{\geq 0}^2$ such that $X_1(t)$, $X_2(t)$ represent the numbers of prey and predators at time $t > 0$, respectively. In our simulation,

$$X(0) = (900, 800)^T, \quad c_1 = 2 \text{ s}^{-1}, \quad c_2 = 0.002 \text{ molec}^{-1}\text{s}^{-1}, \quad c_3 = 2 \text{ s}^{-1}.$$

The fixed stepsize for simulating the SDE part is taken as $\Delta = 0.5$ s. The relative threshold error for partitioning reactions is taken as $\varepsilon = 0.03$, and the reaction set is again repartitioned after every $P = 50$ iterations of updating the state vector.

Figure 4 demonstrates how the proposed algorithm switches back and forth between exact and hybrid diffusion approximation depending on the state of the system. As in the case of Michaelis-Menten kinetics, the accuracy of our hybrid diffusion algorithm is evident from Figure 5 which compares the probability distributions and the corresponding Q-Q plots obtained from the exact Gillespie’s algorithm and Algorithm 1.

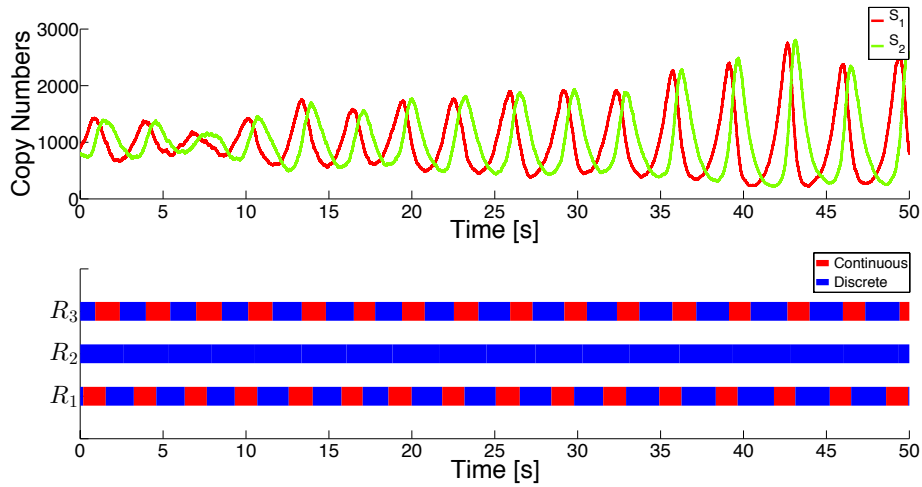


Figure 4: Upper Panel: A single realization of the Lotka-Volterra model when the fast reactions are modeled by diffusion approximation. Lower Panel: Figure depicting the portions of time when a reaction is treated as fast (continuous) or slow (discrete) as dictated by the error bound (3.14).

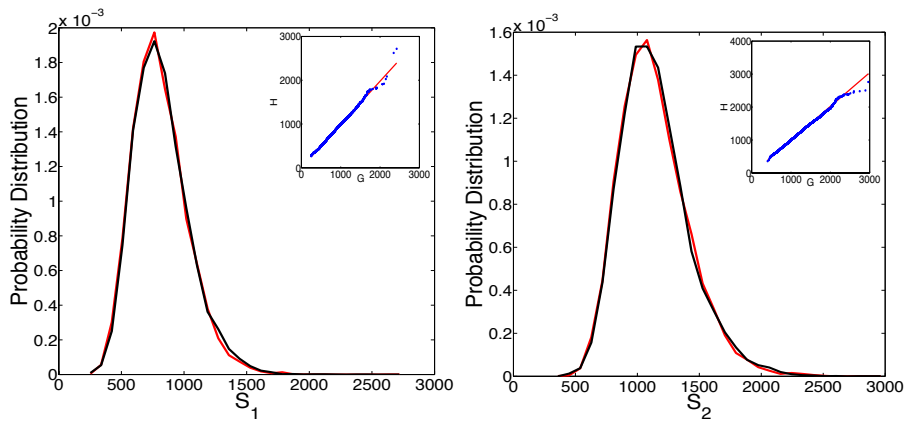


Figure 5: Probability distributions of S_1 (left) and S_2 (right) at $t = 15s$ from 15000 samples constructed with (i) the Gillespie's algorithm (black line) and by (ii) the hybrid diffusion algorithm (red line). Insets show Q-Q plot of 15000 samples comparing the Gillespie's algorithm (G) and the hybrid diffusion algorithm (H).

6.4 The MAPK Pathway and Gene Expression Model

The MAPK (Mitogen Activated Protein Kinase) pathway is one of the most studied signal transduction mechanism that can be observed in all eukaryotic cells. MAPK cascade conveys external signals from the cell membrane to the nucleus and regulates many cellular processes such as proliferation, differentiation, survival and motility. The basic structure of a MAPK cascade consists of three kinases which are the kinase kinase MAPKKK, the kinase MAPKK, and the final kinase MAPK. The signaling process is initiated with a G – protein which transmits the signal to MAPKKK. Phosphorylated MAPKKK phosphorylates MAPKK which activates MAPK. Kinase activation is defined by two reactions in analogy to the Michaelis-Menten model of Section 6.1. The first reaction is a reversible reaction which expresses the binding of a kinase to its substrate to form a complex, and the second reaction converts this complex to a kinase and an activated substrate. (see [26, 27, 29, 30, 34] and the references therein) .

Each MAPK cascade is named according to their MAPK components [30]. In this paper, we will study the ERK (Extracellular Signal Regulated Kinase) pathway which includes Ras as a G – protein, Raf as MAPKKK, MEK as MAPKK and ERK as MAPK [26]. In our model, the process is initiated with Ras – GTP which is the active form of Ras. It binds to Raf to form Raf : Ras – GTP complex which in turn forms Raf_P (phosphorylated Raf). Raf_P binds MEK, MEK_P to form MEK_P, MEK_{PP}, respectively. Finally, MEK_{PP} binds ERK and ERK_P to form ERK_P and ERK_{PP} respectively. Phosphatases, namely Pase1, Pase2 and Pase3 deactivate Raf_P, deactivate MEK's (i.e. MEK_P, MEK_{PP}) and deactivate ERK's (i.e. ERK_P, ERK_{PP}), respectively.

The aim of the ERK signaling pathway is to transform extracellular signals into intracellular signals and finally into a gene regulatory response. External stimulus activates a cell surface receptor which in turn initiates the ERK pathway in the cell. The transcriptional factor ERK_{PP} can then change a target gene from an inactive form GENE_{off} to an active form GENE_{on}. For this reason, in our model, the reaction rate of the activation reaction, $d_{21}(t)$, is defined as $d_{21}(t) = d_{21}^0 + d_{21}^1 [\text{ERK}_{PP}(t)]$, where d_{21}^0 , d_{21}^1 are constants and $[\text{ERK}_{PP}(t)]$ denotes the concentration of ERK_{PP} at time t . The active gene leads to the production of mRNA (transcription) and mRNA is further processed into a Protein through the process of translation. The increase in the number of target Protein corresponds to the cellular response to the initial extracellular signal (see Figure 6A) [24] .

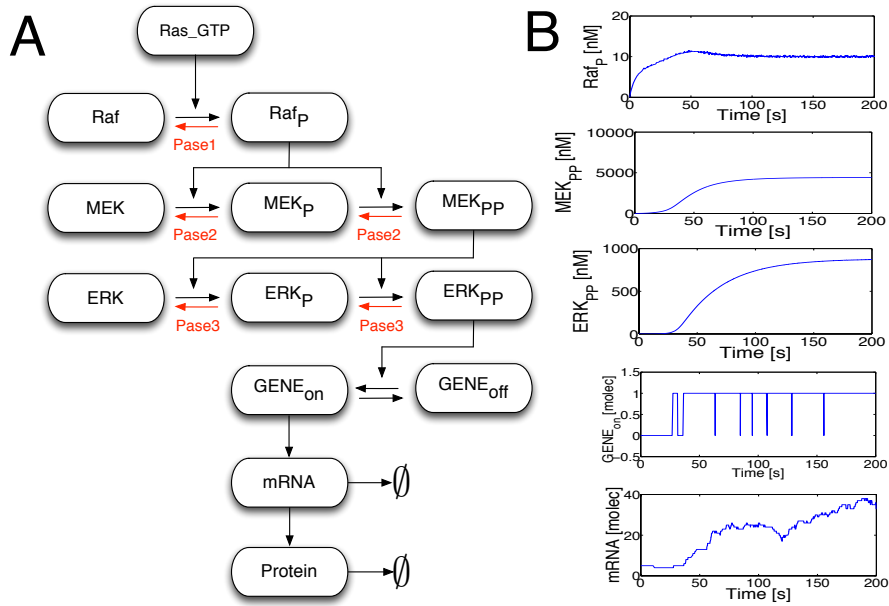


Figure 6: (A) Systematic representation of MAPK pathway and its coupled gene expression. (B) Concentrations of the species Raf_P , MEK_{PP} , ERK_{PP} and the copy numbers of $GENE_{on}$, mRNA in $t \in [0, 200]$ s when R_1, \dots, R_{20} reactions in Table 1 are considered as fast reactions and simulated by diffusion approximation while R_{21}, \dots, R_{25} are considered as slow reactions and Markov chain formulation is kept.

This is a typical realistic example in modeling coupled cellular processes in systems of biology. Due to the combination of fast, high-copy signal transduction with slow, low copy gene expression dynamics this is a typical multi-scale, stiff problem for which our hybrid algorithm is designed for. The complete list of reactions and the reaction rate constants in $[s^{-1}]$ and $[molec^{-1}s^{-1}]$ for unimolecular and bimolecular reactions, respectively, for that model are given in Table 1. The reactions and their rates are taken from [4].

Reactions	Stochastic rate constants
$R_1 : \text{Ras} - \text{GTP} + \text{Raf} \xrightleftharpoons[c_1]{d_1} \text{Raf} : \text{Ras} - \text{GTP}$	$c_1 = 5e - 06 \text{ molec}^{-1} \text{ s}^{-1}$ $d_1 = 0.0053 \text{ s}^{-1}$
$R_2 : \text{Raf} : \text{Ras} - \text{GTP} \xrightarrow{c_2} \text{Ras} - \text{GTP} + \text{Raf}_P$	$c_2 = 3.1 \text{ s}^{-1}$
$R_3 : \text{Raf}_P + \text{Pase1} \xrightleftharpoons[c_3]{d_3} \text{Raf}_P : \text{Pase1}$	$c_3 = 6e - 05 \text{ molec}^{-1} \text{ s}^{-1}$ $d_3 = 1.41589e - 04 \text{ s}^{-1}$
$R_4 : \text{Raf}_P : \text{Pase1} \xrightarrow{c_4} \text{Raf} + \text{Pase1}$	$c_4 = 3.16228 \text{ s}^{-1}$
$R_5 : \text{Raf}_P + \text{MEK} \xrightleftharpoons[c_5]{d_5} \text{Raf}_P : \text{MEK}$	$c_5 = 1.07e - 05 \text{ molec}^{-1} \text{ s}^{-1}$ $d_5 = 0.033 \text{ s}^{-1}$
$R_6 : \text{Raf}_P : \text{MEK} \xrightarrow{c_6} \text{Raf}_P + \text{MEK}_P$	$c_6 = 1.9 \text{ s}^{-1}$
$R_7 : \text{MEK}_P + \text{Pase2} \xrightleftharpoons[c_7]{d_7} \text{MEK}_P : \text{Pase2}$	$c_7 = 4.74801e - 08 \text{ molec}^{-1} \text{ s}^{-1}$ $d_7 = 0.252982 \text{ s}^{-1}$
$R_8 : \text{MEK}_P : \text{Pase2} \xrightarrow{c_8} \text{MEK} + \text{Pase2}$	$c_8 = 0.112387 \text{ s}^{-1}$
$R_9 : \text{Raf}_P + \text{MEK}_P \xrightleftharpoons[c_9]{d_9} \text{Raf}_P : \text{MEK}_P$	$c_9 = 1.07e - 05 \text{ molec}^{-1} \text{ s}^{-1}$ $d_9 = 0.033 \text{ s}^{-1}$
$R_{10} : \text{Raf}_P : \text{MEK}_P \xrightarrow{c_{10}} \text{Raf}_P + \text{MEK}_{PP}$	$c_{10} = 0.8 \text{ s}^{-1}$
$R_{11} : \text{MEK}_{PP} + \text{ERK} \xrightleftharpoons[c_{11}]{d_{11}} \text{MEK}_{PP} : \text{ERK}$	$c_{11} = 8.85125e - 07 \text{ molec}^{-1} \text{ s}^{-1}$ $d_{11} = 0.01833 \text{ s}^{-1}$
$R_{12} : \text{MEK}_{PP} : \text{ERK} \xrightarrow{c_{12}} \text{MEK}_{PP} + \text{ERK}_P$	$c_{12} = 0.028 \text{ s}^{-1}$
$R_{13} : \text{ERK}_{PP} + \text{Pase3} \xrightleftharpoons[c_{13}]{d_{13}} \text{ERK}_{PP} : \text{Pase3}$	$c_{13} = 3.9739e - 04 \text{ molec}^{-1} \text{ s}^{-1}$ $d_{13} = 5 \text{ s}^{-1}$
$R_{14} : \text{ERK}_{PP} : \text{Pase3} \xrightarrow{c_{14}} \text{ERK}_P + \text{Pase3}$	$c_{14} = 0.0076 \text{ s}^{-1}$
$R_{15} : \text{MEK}_{PP} + \text{Pase2} \xrightleftharpoons[c_{15}]{d_{15}} \text{MEK}_{PP} : \text{Pase2}$	$c_{15} = 2.37e - 05 \text{ molec}^{-1} \text{ s}^{-1}$ $d_{15} = 0.79 \text{ s}^{-1}$
$R_{16} : \text{MEK}_{PP} : \text{Pase2} \xrightarrow{c_{16}} \text{MEK}_P + \text{Pase2}$	$c_{16} = 0.112387 \text{ s}^{-1}$
$R_{17} : \text{MEK}_{PP} + \text{ERK}_P \xrightleftharpoons[c_{17}]{d_{17}} \text{MEK}_{PP} : \text{ERK}_P$	$c_{17} = 8.85125e - 06 \text{ molec}^{-1} \text{ s}^{-1}$ $d_{17} = 0.01833 \text{ s}^{-1}$
$R_{18} : \text{MEK}_{PP} : \text{ERK}_P \xrightarrow{c_{18}} \text{MEK}_{PP} + \text{ERK}_{PP}$	$c_{18} = 0.701662 \text{ s}^{-1}$
$R_{19} : \text{ERK}_P + \text{Pase3} \xrightleftharpoons[c_{19}]{d_{19}} \text{ERK}_P : \text{Pase3}$	$c_{19} = 8.33e - 07 \text{ molec}^{-1} \text{ s}^{-1}$ $d_{19} = 0.25 \text{ s}^{-1}$
$R_{20} : \text{ERK}_P : \text{Pase3} \xrightarrow{c_{20}} \text{ERK} + \text{Pase3}$	$c_{20} = 0.0076 \text{ s}^{-1}$
$R_{21} : \text{GENE}_{\text{on}} \xrightleftharpoons[c_{21}]{d_{21}} \text{GENE}_{\text{off}}$	$c_{21} = 0.05 \text{ s}^{-1}$ $d_{21}(t) = 0.01 + 0.003 [\text{ERK}_{PP}(t)] \text{ s}^{-1}$
$R_{22} : \text{GENE}_{\text{on}} \xrightarrow{c_{22}} \text{GENE}_{\text{on}} + \text{mRNA}$	$c_{22} = 0.5 \text{ s}^{-1}$
$R_{23} : \text{mRNA} \xrightarrow{c_{23}} \text{mRNA} + \text{Protein}$	$c_{23} = 0.3 \text{ s}^{-1}$
$R_{24} : \text{mRNA} \xrightarrow{c_{24}} \emptyset$	$c_{24} = 0.015 \text{ s}^{-1}$
$R_{25} : \text{Protein} \xrightarrow{c_{25}} \emptyset$	$c_{25} = 5e - 06 \text{ s}^{-1}$

Table 1: Reactions and rate parameters for the ERK signal gene expression pathway.

In our application, we will fix the concentrations of reactants of the MAPK cascade and the copy numbers of reactants of the gene expression. Therefore, for the sake of simplicity, we define the state vector as $X(t) = (X_{\text{MAPK}}(t), X_{\text{GENE}}(t))^T$ where

$$\begin{aligned} X_{\text{MAPK}}(t) = & (\text{Ras} - \text{GTP}, \text{Raf}, \text{Raf} : \text{Ras} - \text{GTP}, \text{Raf}_P, \text{Pase1}, \\ & \text{Raf}_P : \text{Pase1}, \text{MEK}, \text{Raf}_P : \text{MEK}, \text{MEK}_P, \\ & \text{Pase2}, \text{MEK}_P : \text{Pase2}, \text{Raf}_P : \text{MEK}_P, \text{MEK}_{PP}, \text{ERK}, \\ & \text{MEK}_{PP} : \text{ERK}, \text{ERK}_P, \text{ERK}_{PP}, \text{MEK}_{PP} : \text{ERK}_P, \\ & \text{Pase3}, \text{ERK}_P : \text{Pase3}, \text{MEK}_{PP} : \text{Pase2}, \text{ERK}_{PP} : \text{Pase3}), \end{aligned}$$

$X_{\text{GENE}}(t) = (\text{GENE}_{\text{on}}, \text{GENE}_{\text{off}}, \text{mRNA}, \text{Protein})$. To convert the amount of species of the components $X(t)$ from copy numbers to nanomolar [nM] concentrations, we use the relation

$$U(t) = X(t)/n_A\Omega, \quad (6.35)$$

where $n_A = 6 \times 10^{23}$ represents the Avogadro's number and Ω is the volume of the reaction compartment in liters [33]. A complete list of initial number of molecules and corresponding initial concentrations can be seen in Table 2.

Species	Copy numbers	Concentrations [nM]
Ras – GTP	10000	16.6667
Raf	711081	1185.135
Raf : Ras – GTP	11	0.0183
Raf _P	11	0.0183
Pase1	49990	83.3167
Raf _P : Pase1	10	0.0167
MEK	2830668	4717.78
Raf _P : MEK	173	0.2883
MEK _P	185198	308.6633
Pase2	121372	202.2867
MEK _P : Pase2	2921	4.8683
Raf _P : MEK _P	26	0.0433
MEK _{PP}	59	0.0983
ERK	685746	1142.91
MEK _{PP} : ERK	768	1.28
ERK _P	5275	8.7917
ERK _{PP}	27	0.045
MEK _{PP} : ERK _P	0	0
Pase3	165519	275.865
ERK _P : Pase3	2823	4.705
MEK _{PP} : Pase2	187	0.3167
ERK _{PP} : Pase3	360	0.6
GENE _{on}	0	0
GENE _{off}	1	0.0017
mRNA	5	0.0083
Protein	0	0

Table 2: Species initial copy numbers and corresponding concentrations for the nominal volume of the reaction compartment of $\Omega = 10^{-12}$ in liters .

According to the reactions in Table 1, the following 8 conservation laws can be

identified:

$$\begin{aligned}
C_1 &= \text{Ras} - \text{GTP} + \text{Raf} : \text{Ras} - \text{GTP} \\
C_2 &= \text{Raf} + \text{Raf}_P + \text{Raf}_P : \text{MEK} + \text{Raf}_P : \text{Pase1} + \text{Raf}_P : \text{MEK}_P \\
&\quad + \text{Raf} : \text{Ras} - \text{GTP} \\
C_3 &= \text{Pase1} + \text{Raf}_P : \text{Pase1} \\
C_4 &= \text{MEK} + \text{MEK}_P + \text{MEK}_{PP} + \text{MEK}_P : \text{Pase2} \\
&\quad + \text{MEK}_{PP} : \text{ERK} + \text{MEK}_{PP} : \text{Pase2} + \text{MEK}_{PP} : \text{ERK}_P \\
&\quad + \text{Raf}_P : \text{MEK} + \text{Raf}_P : \text{MEK}_P \\
C_5 &= \text{MEK}_P : \text{Pase2} + \text{MEK}_{PP} : \text{Pase2} + \text{Pase2} \\
C_6 &= \text{ERK} + \text{ERK}_P + \text{ERK}_{PP} + \text{ERK}_P : \text{Pase3} \\
&\quad + \text{ERK}_{PP} : \text{Pase3} + \text{MEK}_{PP} : \text{ERK} + \text{MEK}_{PP} : \text{ERK}_P \\
C_7 &= \text{ERK}_P : \text{Pase3} + \text{ERK}_{PP} : \text{Pase3} + \text{Pase3} \\
C_8 &= \text{GENE}_{\text{on}} + \text{GENE}_{\text{off}}.
\end{aligned}$$

Here, C_1, C_2, \dots, C_8 are mass conservation constants. Since the number of molecules of MAPK signaling cascade, $X_{\text{MAPK}}(t)$ are high, we expect R_1, \dots, R_{20} reactions in Table 1 will be fast reactions while R_{21}, \dots, R_{25} will be slow reactions. Concentrations of Raf_P , MEK_{PP} , ERK_{PP} and the copy numbers of GENE_{on} , mRNA when R_1, \dots, R_{20} reactions in Table 1 are considered as continuous reactions and modeled by diffusion approximation while R_{21}, \dots, R_{25} are considered as slow reactions and modeled by Markov jump process in time interval $[0, 200]$ s can be seen in Figure 6B. This figure demonstrates the amounts of some species when static partitioning algorithm is applied. We also implement dynamic partitioning algorithm to the model and compare the computation time of Algorithm 1 with that of Gillespie's direct method for different volumes of the reaction compartment Ω . In our application, we consider the volume of the cell compartment where the signaling reactions take place, is scaled with a positive constant ω such that $\Omega = \omega V$ where $V = 10^{-12}$ is the nominal cell volume in liters [33] while the sub-compartment where the gene expression reactions take place is fixed for all Ω values. We consider concentrations of the reactants of the MAPK cascade, $X_{\text{MAPK}}(t)$, and the number of molecules of species of the gene expression, $X_{\text{GENE}}(t)$, are same for all volumes (see Table 2). Hence, to keep same concentrations for all volumes, we multiply the number of molecules of the components $X_{\text{MAPK}}(t)$ with ω if the volume of the reaction compartment is $\Omega = \omega V$. Also, it must be noticed that the stochastic rate constants of bimolecular reactions are divided by ω when the volume of reaction compartment is $\Omega = \omega V$. In Table 3, one can see the CPU times of our algorithm (see Algorithm 1) and Gillespie's direct method in seconds for a single realization of the model in time interval $[0, 10]$ s with $\Delta = 2$ s, $\varepsilon = 0.3$, $P = 20$ for $\omega = 1, 2, 5, 10, 10^2, 10^4, 10^6, 10^8$. To obtain the numerical solution of SDEs, we automatically choose the stepsize of Runge-Kutta method as explained in Section 4 with absolute and relative tolerances of 10^{-12} and 10^{-9} , respectively. Since both the drift, the diffusion term of SDE given by (4.24) are volume dependent, the CPU time of the hybrid diffusion algorithm decreases as expected when the volume increases. Types of

reactions according to Algorithm 1 for $\omega = 1$ can be seen in Figure 7. As discussed before, to preserve the same concentration of species for all volumes, we have to multiply the number of molecules of some species with ω to observe the dynamics for volume $\Omega = \omega V$. This will make a significant change on the CPU time of the Gillespie's algorithm. Since application of the Gillespie's direct method is too time consuming for large volumes, we compute its CPU time only for $\omega = 1, 2, 5, 10$. The results reveal that the hybrid diffusion algorithm significantly reduce the computational time.

ω	CPU Time in seconds	
	Algorithm 1	Gillespie's Direct Method
1	498.82	2872.02
2	498.080	6264.26
5	404.36	15613.46
10	345.41	31356.38
10^2	337.01	—
10^4	167.61	—
10^6	119.93	—
10^8	78.21	—

Table 3: The CPU times (in seconds) of the Algorithm 1 and the Gillespie's direct method for the MAPK cascade together with its gene expression. For all volumes, we have the same concentrations of the MAPK cascade species and the same copy numbers for species of gene expression. To preserve the same concentration of MAPK species, we multiply their number of molecules with ω to observe the dynamics of the model in the reaction compartment with volume $\Omega = \omega V$ where $\Delta = 2s$, $\varepsilon = 0.3$, $P = 20$ in $t \in [0, 10]$ s.

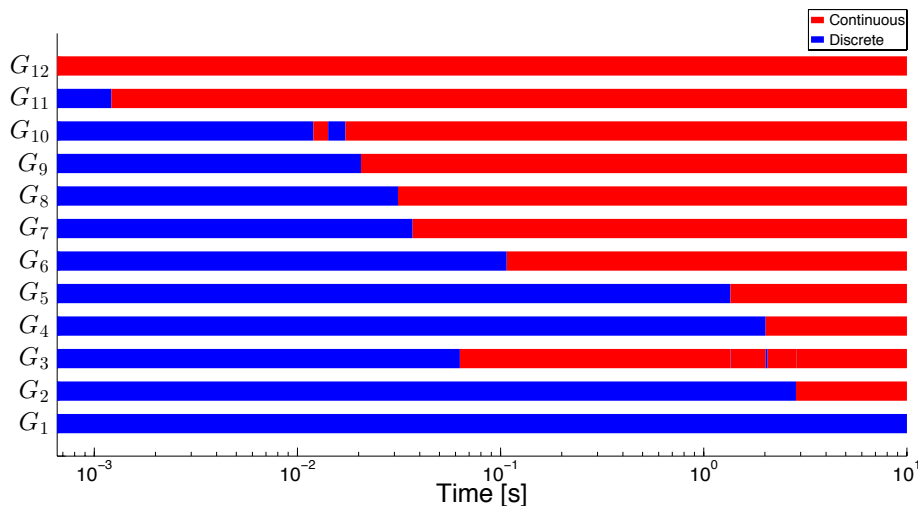


Figure 7: Depicts the portions of time when reactions of the MAPK signaling pathway are treated as fast or slow in the time interval $[0, 10]$ s according to our dynamic partitioning algorithm with $\Delta = 2$ s, $\varepsilon = 0.3$, $P = 20$ and $\omega = 1$. Since the number of reactions is too high, to have a better visualization we group the reactions and also note that x-axis represents the $\log(t)$ of time $t > 0$. Here, $G_1 = (R_{21}^+, R_{21}^-, R_{22}, R_{23}, R_{24}, R_{25})$, $G_2 = R_{18}$, $G_3 = (R_{13}^+, R_{13}^-)$, $G_4 = (R_{17}^+, R_{17}^-)$, $G_5 = R_3^-$, $G_6 = R_3^+$, $G_7 = R_9^+$, $G_8 = (R_4, R_{10})$, $G_9 = (R_2, R_5^+)$, $G_{10} = R_6$, $G_{11} = (R_1^+, R_1^-)$, $G_{12} = (R_5^-, R_7^+, R_8, R_9^-, R_{11}^+, R_{11}^-, R_{12}, R_{14}, R_{15}^+, R_{15}^-, R_{16}, R_{19}^+, R_{19}^-, R_{20})$ where R_i^+ denotes the forward reaction (\rightarrow) while R_i^- denotes the backward reaction (\leftarrow) for $i = 1, 2, \dots, 25$.

7 Conclusion

In this work, we developed techniques for simulating certain multi-scale reaction systems more efficiently. Our strategy involved a systematic approach of separating the reactions into fast and slow groups. The fast reactions are simulated by a diffusion approximation while the exact Gillespie-type simulation procedure is maintained for the slow ones. The partitioning of the reaction set is based on an appropriate error bound whose derivation is one of the central themes of the paper. The theoretical results are then effectively encoded in an efficient fast algorithm which also allows for the partition to change dynamically over the course of time.

The paper used Runge-Kutta integration methods to approximate the solutions of SDEs. Also the conservation relations, occurring naturally in many reaction models, have been properly utilized to reduce the dimensionality of the corresponding SDEs and to ensure strict mass conservation.

The proposed algorithms are implemented for the well-known Michaelis-Menten kinetics, the Lotka-Volterra system and a realistic MAPK cascade together with its gene

expression. The results reveal that the proposed algorithm simulates the multi-scale processes with a significant gain in runtime but little loss in accuracy when compared to the exact Gillespie algorithm.

8 Acknowledgement

Funding D. Altıntan acknowledges the support from the Scientific and Technological Research Council of Turkey (TÜBİTAK), grant no. 2219.

References

- [1] A. Alfonsi, E. Cancès, G. Turinici, B.D. Ventura, and W. Huisinga. Adaptive simulation of hybrid stochastic and deterministic models for biochemical systems. In *ESAIM: Proc.*, volume 14, pages 1–13, 2005.
- [2] D.F. Anderson and T.G. Kurtz. Continuous time markov chain models for chemical reaction networks. In H. Koepl, G. Setti, M. di Bernardo, and D. Densmore, editors, *Design and Analysis of Biomolecular Circuits*. Springer-Verlag, 2011.
- [3] K. Burrage and P.M. Burrage. High strong order explicit Runge-Kutta methods for stochastic ordinary differential equations. *Applied Numerical Mathematics*, 22:81–101, 1996.
- [4] W.W. Chen, B. Schoeberl, P.J. Jasper, M. Niepel, U.B. Nielsen, and D.A. Lauffenburger. Input–output behavior of ErbB signaling pathways as revealed by a mass action model trained against dynamic data. *Molecular Systems Biology*, 5(239), 2009.
- [5] A. Cornish-Bowden and J.-H.S. Hofmeyr. The role of stoichiometric analysis in studies of metabolism : An example. *Journal of Theoretical Biology*, 216:179–191, 2002.
- [6] A. Coulon, C. C. Chow, R. H. Singer, and D. R. Larson. Eukaryotic transcriptional dynamics: from single molecules to cell populations molecules to cell populations. *Nature Reviews Genetics*, 14:572–584, 2013.
- [7] A. Crudu, A. Debussche, and O. Radulescu. Hybrid stochastic simplifications for multiscale gene networks. *BMC Systems Biology*, 3(89), 2009.
- [8] A. Eldar and M. B. Elowitz. Functional roles for noise in genetic circuits. *Nature*, 467:167–173, 2010.
- [9] S. N. Ethier and T. G. Kurtz. *Markov processes*. Wiley Series in Probability and Mathematical Statistics: Probability and Mathematical Statistics. John Wiley & Sons, Inc., New York, 1986. Characterization and convergence.

- [10] N. Friedman, L. Cai, and X.S. Xie. Stochasticity in gene expression as observed by single-molecule experiments in live cells. *Israel Journal of Chemistry*, 49:333–342, 2010.
- [11] M.A. Gibson and J. Bruck. Efficient exact stochastic simulation of chemical systems with many species and many channels. *The Journal of Physical Chemistry A*, 104(9):1876–1889, 2000.
- [12] D.T. Gillespie. A rigorous derivation of the chemical master equation. *Physica A*, 188:404–425, 1992.
- [13] E. Hairer, C. Lubich, and G. Wanner. *Geometric Numerical Integration — Structure-Preserving Algorithms for Ordinary Differential Equations*. Springer Series in Computational Mathematics. Springer-Verlag, New York, 2 edition, 2006.
- [14] E. Hairer, S.P. Nørsett, and G. Wanner. *Solving Ordinary Differential Equations I: Nonstiff Problems*. Springer Series in Computational Mathematics. Springer-Verlag, Berlin Heidelberg, second revised editions edition, 1993.
- [15] E. Hairer and G. Wanner. *Solving Ordinary Differential Equations II: Stiff and Differential-Algebraic Problems*. Springer-Verlag, Berlin Heidelberg, second revised edition edition, 1996.
- [16] E.L. Haseltine and J.B. Rawlings. Approximate simulation of coupled fast and slow reactions for stochastic chemical kinetics. *Journal of Chemical Physics*, 117(15):6959–6969, 2002.
- [17] J. Hasenauer, V. Wolf, A. Kazeroonian, and F. J. Theis. Method of conditional moments (MCM) for the chemical master equation : A unified framework for the method of moments and hybrid stochastic-deterministic models. *Journal of Mathematical Biology*, 2013.
- [18] A. Hellander and P. Lötstedt. Hybrid method for the chemical master equation. *Journal of Computational Physics*, 227(1):100–122, 2007.
- [19] T.A. Henzinger, L. Mikeev, M. Mateescu, and V. Wolf. Hybrid numerical solution of the chemical master equation. In *Proceedings of the 8th International Conference on Computational Methods in Systems Biology*, 8th international Conference on Computational Methods in Systems Biology, pages 55–65. ACM, New York, 2010.
- [20] T. Jahnke. On reduced models for the chemical master equation. *Multiscale Modeling and Simulation*, 9(4):1646–1676, 2011.
- [21] T. Jahnke and M. Kreim. Error bound for piecewise deterministic process modelling stochastic reaction systems. *Multiscale Modeling and Simulation*, 10(4):1119–1147, 2012.

- [22] H.W. Kang and T.G. Kurtz. Separation of time-scales and model reduction for stochastic reaction networks. *Annals of Applied Probability*, 23(2):529–583, 2013.
- [23] Hye-Won Kang, Thomas G. Kurtz, and Lea Popovic. Central limit theorems and diffusion approximations for multiscale Markov chain models. *Ann. Appl. Probab.*, 24(2):721–759, 2014.
- [24] E. Klipp, W. Liebermeister, C. Wierling, A. Kowald, H. Lehrach, and R. Herwig. *Systems Biology: A Textbook*. WILEY - VCH Verlag GmbH & Co. KGaA, 2009.
- [25] P.E. Kloeden and E. Platen. *Numerical Solution of Stochastic Differential Equations*. Springer, Berlin, 1992.
- [26] W. Kolch. Meaningful relationship: the regulation of Ras/ Raf/ MEK/ ERK pathway by protein interactions. *Biochemical Journal*, 351:289–305, 2000.
- [27] W. Kolch, M. Calder, and D. Gilbert. When kinases meet mathematics: the systems biology of mapk signalling. *FEBS Letters*, 579:1891–1895, 2005.
- [28] S. Menz, J.C. Latorre, C. Schütte, and W. Huisinga. Hybrid stochastic–deterministic solution of the chemical master equation. *Multiscale Modeling and Simulation*, 10(4):1232–1262, 2012.
- [29] R.J. Orton, O.E. Sturm, V. Vyshemirsky, M. Calder, D.R. Gilbert, and W. Kolch. Computational modelling of the receptor-tyrosine-kinase-activated MAPK pathway. *Biochemical Journal*, 392:249–261, 2005.
- [30] H. Rubinfeld and R. Seger. The ERK cascade: a prototype of MAPK signaling. *Molecular Technology*, 31:151–174, 2005.
- [31] H. Salis and Y. Kaznessis. Accurate hybrid stochastic simulation of a system of coupled chemical or biochemical reactions. *The Journal of Chemical Physics*, 122:054103, 2005.
- [32] H.M. Sauro and B. Ingalls. Conservation analysis in biochemical networks computational issues for software writers. *Biophysical Chemistry*, 109:1–15, 2004.
- [33] B. Schoeberl, E.A. Pace, J.B. Fitzgerald, B.D. Harms, L. Xu, L. Nie, A. Kalra, V. Paragas, R. Bukhalid, V. Grantcharova, N. Kohli, K.A. West, M. Leszczyniecka, M.J. Feldhaus, A.J. Kudla, and U.B. Nielsen. Therapeutically targeting ErbB3: A key node in ligand-induced activation of the ErbB receptor-PI3K axis. *Science Signaling*, 2(77), 2009.
- [34] T. Tian and J. Song. Mathematical modelling of the MAP kinase pathway using proteomic datasets. *PLOS*, 7(8):e42230, 2002.
- [35] J. Yu, J. Xiao, X. Ren, K. Lao, and X.S. Xie. Probing gene expression in live cells, one protein molecule at a time. *Science*, 311(5767):1600–1603, 2006.